Lithology constraints from seismic waveforms: application to opal-A to opal-CT transition

by

Mohammad Maysami

B.Sc., Sharif University of Technology, 2005

A THESIS SUBMITTED IN PARTIAL FULFILMENT OF
THE REQUIREMENTS FOR THE DEGREE OF

MASTER OF APPLIED SCIENCE

in

The Faculty of Graduate Studies

(Geophysics)

THE UNIVERSITY OF BRITISH COLUMBIA

February 2008

Abstract

In this work, we present a new method for seismic waveform characterization, which is aimed at extracting detailed litho-stratigraphical information from seismic data. We attempt to estimate the lithological attributes from seismic data according to our parametric representation of stratigraphical horizons, where the parameter values provide us with a direct link to nature of lithological transitions. We test our method on a seismic dataset with a strong diagenetic transition (opal-A to opal-CT transition). Given some information from cutting samples of well, we use a percolation-based model to construct the elastic profile of lithological transitions. Our goal is to match parametric representation for the diagenetic transition in both real data and synthetic data given by these elastic profiles. This match may be interpreted as a well-seismic tie, which reveals lithological information about stratigraphical horizons.

Table of Contents

List of Figures

Acknowledgements

First and foremost, I would like to express my sincere gratitude to my supervisor, Dr. Felix J. Herrmann, for his great insight and wise guidance throughout this research project. His serious research attitude will always inspire me all my life.

My sincere thanks are also due to Dr. Oldenburg, Dr. Bostock, and Dr. Greif for their constructive suggestions as members of my thesis committee. Their kindness and word of wisdom have always been the sources of enlightenment to me.

I am also deeply indebted to Dr.Henryk Modzelewski for his great advice and assistance regarding the computational and technical problems. I am genuinely grateful to other SLIM (Seismic Laboratory for Imaging and Modeling) team members for being there to help with any problems that I encountered while studying there. Their intelligence, persistence and kindness made my stay at the University of British Columbia stimulating and enjoyable.

My wonderful parents deserve thanks for all the love they have given me and for always being so supportive and proud. I would like to thank my kind and loving sisters, whose altruism and compassion are inspiring.

The authors also thank David Wilkinson for constructive discussions about this research. Veritas DGC Company is gratefully thanked for the real datasets. This work was in part financially supported by NSERC Discovery Grant 22R81254 and CRD Grant DNOISE 334810-05 of Felix J. Herrmann and was carried out as part of the CHARM project with support, secured through Chevron.

To my parents,

who taught me how to love and how to be loved.

Chapter 1

Introduction

In this study, we propose a novel method to identify and quantify generalized lithological transitions, as long as their scale is above the seismic wavelength. In this method, we link the seismic waveforms to fractional-order transitions through a parametric waveform inversion process. By using the percolation model proposed by Herrmann and Bernabé (2004), we show that smooth changes (connectivity) in lithology may also give rise to a seismic reflection. Consequently, a wider range of lithological transitions in depositional environments, which is not given by other methods, exists in our model. The primary goals of this study are to answer two general questions: 1) is the waveform quantification coherent with the stratigraphical structure of seismic data; and 2) can we find a direct link between our quantification of seismic waveforms and nature of associated lithological boundaries? A positive answer to these question means that we have a tool, which provides us with increased insight into litho-stratigraphy structure of the subsurface.

Seismic surveys are a valuable tool to extract geological structure of the lithological boundaries in the subsurface. However, this method only images seismic reflectors and does not provide precise information on the associated lithological transitions directly. Therefore, there is a crucial step in seismic imaging where observations are translated into models of the Earth structure that are geologically valid. Using these models, we can extract the geological and stratigraphical features of the subsurface. Transitions in the lithology are examples of these geological features, which are mathematically represented by zero-order discontinuities (step functions) or first-order ramp functions in most cases. However, multiscale analysis on well and seismic data (Muller et al., 1992; Herrmann, 1997, 1998) showed that these representations may not be rich enough to describe the different types of transitions present in sedimentary basins. In reality, seismically-observed reflectors correspond to complex lithological changes typically composed of sub-wavelength features or more gradational lithological transitions. Consequently, valuable information is lost by assuming these transitions to be given by step or ramp discontinuities. Instead, multiscale analysis on sedimentary records revealed the existence of transitions with varying singular-

ity orders (Herrmann, 1998, 2001; Herrmann et al., 2001; Herrmann, 2005). Singularities are points in a signal at which the derivative is undefined. This generalized type of fractional-order singularity is given by fractionally differentiating/integrating a zero-order discontinuity (see Fig. 1.1(a) for a schematic of fractional-order transitions). Lithological transitions have been studied from various perspectives. However, most of available models for lithological transitions lack a straightforward generalization to fractional-order transitions.

Lithological perspective: Classical seismic stratigraphical models (Payton, 1977; Harms and Tackenberg, 1972) represent sub-wavelength lithology variation by multiple zero-order and first-order discontinuities. The simplicity of this assumption limits the ability of these models to constrain the lithological structure. In that sense, fractional-order transitions provide a more accurate parametric description to describe acoustic impedance profiles across the transitions by eliminating the superposition of multiple reflectors. In this perspective, variations in the acoustic impedance are interpreted as proxies for the lithology, e.g., observed seismic waveforms are through complex-trace attributes related to fining upward or coarsening upward sequences as shown in Herrmann et al. (2001).

Even though the above extension of transition models is proved to be useful, two important aspects are missing, namely (i) a first principal rock-physical model that predicts the occurrence of fractional-order transitions as a function of a smoothly varying lithology/composition and, (ii) a robust estimation technique, extracting information on the transition order from bandwidth limited seismic traces. In order to make prospect towards these two aspects, we have to include more careful considerations regarding the rock-physical and seismological aspects of our problem.

Rock-physical perspective: In this thesis, we look at how changes in the rock-physical properties, such as the rock's acoustic wave speed and density, are related to the volume fractions of a bi-compositional rock, e.g., a rock consisting of a sand-shale or opal-A/CT mixture. From the rock-physical perspective, transitions are described with their elastic profiles, e.g., velocity and density.

In this case, the traditional Hashin-Shtrikman (HS) bounds are used to constrain the elastic moduli (see Hashin and Shtrikman (1962) for more details). Even though these bounds have proved to be useful in describing the overall behavior of binary mixtures, this theory does not predict

sharp transitions in the rock properties as a function of the composition. By including the important concept of connectivity amongst the two components of the rock mixture, Herrmann and Bernabé (2004) have introduced a model predicting a critical volume fraction at which the stronger of the two mixing components connects. At that point, the overall strength of the mixture grows with the size of the connected cluster, yielding a fractional-order transition for the seismic velocity. This model (HB model) implies sharp transitions even in cases where the rock's composition and hence the density vary smoothly. Before transgressing the critical point, the velocities predicted by the HB model follows the lower HS-bound, followed by the occurrence of sudden sharp increase in the velocity, which ends up at the velocity predicted by the upper HS-bound.

Seismological perspective: Amongst reflection seismologists, the Earth subsurface is often idealized as a stack of homogeneous layers separated by zero-order discontinuities. This model yields a spiky reflection coefficient sequence for which deconvolution methods have been derived, removing the seismic source signature. Despite recent developments (Saggaf and Robinson, 2000), earth models consisting of a sparse set of different fractional-order transitions render conventional deconvolution techniques ineffective.

In this thesis, we present a two-stage method that handles this more complex situation and during which (i) reflection events are first detected by a multiscale technique deriving from the work by Holschneider (1995), followed by (ii) a nonlinear parametric inversion technique. During the latter, seismic attributes, including the illusive singularity orders, are estimated from seismic waveforms extracted during the multiscale detection.

The thesis is organized as follows. First, we introduce the site percolation model and discuss the seismic response of this model, which we use as the "rock-physics" forward model. We proceed by presenting a seismic waveform characterization method, which first extracts stratigraphical horizons by locating major features in the seismic data and then processes each event with an inversion where it is represented by only a few parameters associated with a parametric waveform. We apply our method to a real data and discuss the results in term of satisfying our expectations. We then aim at recovering the geological details from seismic data by focusing on a diagenetic transition in the data. The percolation model provides us with a synthetic seismic reflector, which is then parametrized and matched to real data. We describe how this tie can provide us with lithological insights from the seismic data.

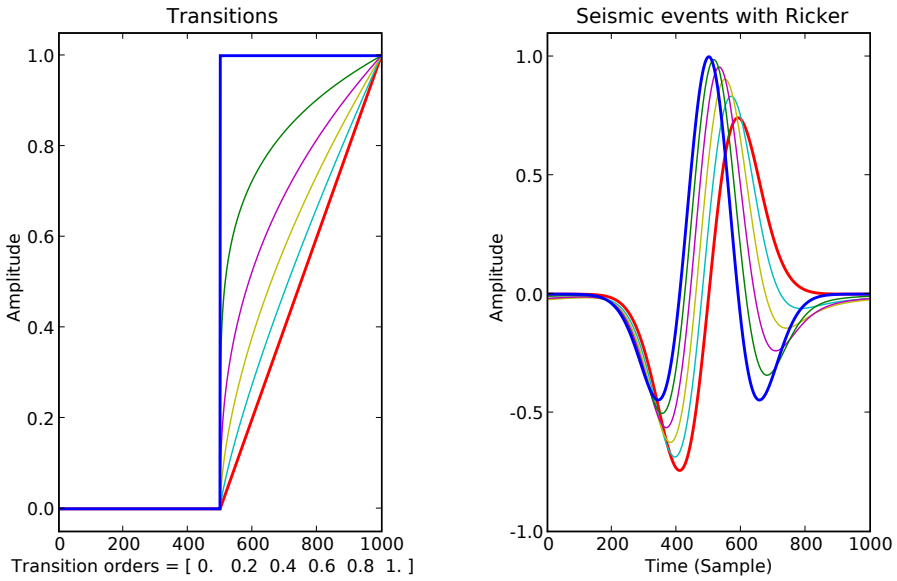

(a) (b)

Figure 1.1: Generalized type of seismic transitions with different singularity orders including fractional-orders **(left)**. Corresponding seismic waveform **(right)** is given by convolving the seismic source function, which is taken to be a Ricker wavelet.

Chapter 2

Rock-physics model

The Earth's subsurface consists of layers of different rock properties separated by transitions. Transitions are regions where the acoustic impedance of the Earth changes rapidly with respect to the seismic wavelength. These sudden variations give rise to the reflection of seismic waves, which creates singularities in the recorded seismic trace. As reported in the literature, while abrupt lithofacies transition give rise to high-order (more sharp) singularities, a more gradual transition leads to low-order (less sharp) singularities. Consequently, singularity orders reflect sharpness of the corresponding lithological boundary (Herrmann et al., 2001). Rock physicists try to impose these lithological constraints on the elastic properties as a function of composition by using different models. Most of these models, however, generally assume that homogeneous mixing of facies can only give rise to smooth and non-singular elastic properties and the existence of the singularities is related to rapid changes in composition only. In recent studies on upper-mantle transitions (Herrmann and Bernabé, 2004), a percolation-based model is proposed, which, unlike the previous models, unravels the sharp changes in seismic velocities across the transitions. Herrmann and Bernabé (2004) predict that the singularity in elastic moduli and hence seismic velocity occurs at a critical volume fraction of end-members of the mixture. The percolation model could explain the nature of various transitions from the properties of rocks. Other than excluding the limitations of the existing models as discussed earlier in the introduction, the model also provides the scale invariance.

2.1 The site percolation model

The site percolation model assumes a simplified bi-compositional model to represent microscale changes along the boundaries of layers. The facies in this binary mixture are divided into a weak lithofacies at the top and a strong lithofacies in the deeper zone. The weak and strong materials are denoted with *WP* and *SP*, respectively. The percolation model applies to the co-existence region where both end-members of the binary mixture are

involved. We assume the volume fraction of strong and weak material, given by p and $q = 1 - p$, respectively, to depend on the vertical coordinate only. While microscopic inclusions in the co-existence region are randomly distributed (see Fig. 2.1(c)), percolation occurs at a threshold, at which the ∞-cluster of SP inclusions is formed. The percolation threshold $p_c = p(z_c)$, which corresponds to a critical depth z_c is denoted by a vertical dashed line in Figure 2.1. The volume fraction p^* of the ∞-cluster is given as

$$p^* = \begin{cases} 0 & \text{if } p < p_c \\ p\ (\frac{p-p_c}{1-p_c})^\beta & \text{if } p \geq p_c \end{cases},$$

where β is a positive real parameter related to the percolation model (see Herrmann and Bernabé (2004) for more details). Accordingly, the elastic moduli given by the model contain a singularity of order β. These moduli give rise to a linear gradient for density of the mixture as well as a wave speed profile, which contains a switch-like singularity at p_c (see Fig. 2.1(a), 2.1(b)). While other models confine the seismic wave velocity in the Hashin-Shtrikman bounds (Hashin and Shtrikman, 1962), the percolation theory predicts a definite velocity profile within those bounds (Mori and Tanaka, 1973; Benveniste, 1987; Luo and Weng, 1987). In our implementation, we have equivalently replaced these bounds with Reuss and Voigt averages (see Fig. 2.1(b)). The velocity change within these bounds is controlled by p_c and β, which are determined by the end-members of the mixture. Consequently, the order β is considered to be independent of the random emplacement of inclusions.

2.2 Seismic response of the percolation model

The convolution model is widely used in seismic processing as a simplified model for the Earth response to the propagation of the seismic wave. Based on this model, the recorded seismic trace at the surface can be written as

$$s(t) \propto (\psi * r)(t), \tag{2.1}$$

where ψ shows the seismic source wavelet and r is the imaged travel-time reflectivity sequence. Figure 1.1(b) shows various seismic waveforms given by the convolution model in presence of fractional-order transitions. Accordingly, what seismic receivers records at the surface, can be thought of as the response of the Earth filtered through the source wavelet. The convolution model uses a simple reflectivity series for modeling the Earth (Yilmaz, 2001)

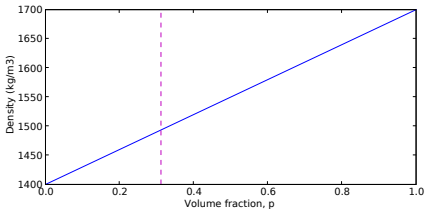

(a)

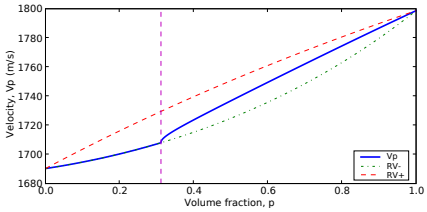

(b)

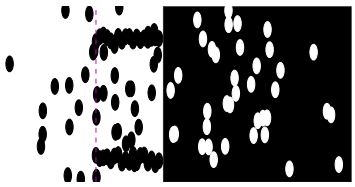

(c)

Figure 2.1: Schematic Site percolation model. **(a)** The mixture density profile, $\rho = q * \rho_{WP} + p * \rho_{SP}$, versus volume fraction in co-existence region. **(b)** Corresponding compressional wave velocity (solid line) with a singularity at p_c as a function of volume fraction. It is bounded with Reuss and Voigt averages shown in dashed lines. The singularity order was taken to be $\beta = 0.41$. **(c)** Illustration of co-existence region. Black and white ellipsoids show inclusions of SP and WP, respectively. At critical volume fraction p_c (dashed vertical lines), SP inclusions percolate and an infinite connected cluster is formed.

in which (i) the subsurface is formed by horizontal layers of constant velocity; (ii) the compressional plane seismic wave impinges on layer boundaries at normal incident angles.

Given elastic properties along transitions by the site percolation model, we can compute the reflection coefficients of normal incident wave, which are related to changes in acoustic impedance (Yilmaz, 2001). Figure 2.2 shows how this model can be applied to a reflectivity series to generate a seismic trace. Combination of the site percolation model and the convolution model forms a forward model that provokes a clarified relation between transitions' nature and waveforms in the seismic trace (events that are triggered by transition regions).

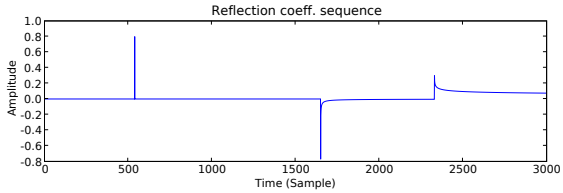

(a)

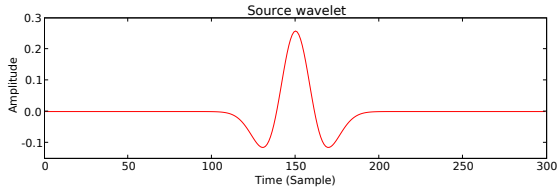

(b)

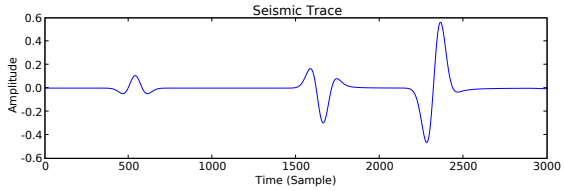

(c)

Figure 2.2: Seismic convolution model; **(a)** Reflection coefficient sequence includes singularities with different signs and orders. **(b)** Seismic source function is taken to be a Ricker wavelet. **(c)** The convolution of reflection coefficients and seismic source function gives the corresponding seismic trace.

2.2.1 The seismic source function

In real world, seismic sources are not ideal spikes. Therefore, we need to have a preliminary knowledge of the seismic source wavelet to obtain the seismic response of the percolation model. However, in most geophysical surveys, the seismic source function ψ is unknown. For our purpose, we assume that the seismic source function has finite smoothness and wiggliness. Combining both conditions can allow us to determine the details of the frequency content of the source function. The first condition is to limit the high-frequency content by setting the asymptotic decay rate for high frequencies. This is imposed by

$$\int_{\mathbb{R}} |\hat{\psi}(\omega)| \ |\omega|^{\gamma} \ d\omega < \infty, \tag{2.2}$$

which means the wavelet is γ-times continuously differentiable, i.e., $\psi \in \mathbf{C}^{\gamma}$. Here, $\hat{\psi}(\omega) = \int_{-\infty}^{+\infty} \psi(t) \ e^{-j\omega t}$ denotes the Fourier transform of ψ. The second condition requires the wavelet ψ to be orthogonal with respect to some finite-order polynomial,

$$\int_{\mathbb{R}} t^{q} \ \psi(x) \ dx = 0 \quad \text{for} \quad 0 \leq q \leq M, \tag{2.3}$$

hence describing its wiggliness. It defines the number of vanishing moments of ψ and rules the differentiability of the Fourier transform at zero frequency. Knowing the source wavelet makes it possible to generate the seismic data using the convolution model.

Chapter 3

Seismic waveform characterization

Here, our aim is two-fold: finding the locations of the reflectors, i.e., delineating the *stratigraphy*, and extracting information on the nature of the transitions. For this purpose, we represent a vertical 1-D profile of the Earth as a weighted superposition of parametrized waveforms

$$s(t) = \sum_{i \in I} c_i \ \psi_{\sigma_i}^{\alpha_i}(t - \tau_i) \ e^{j\pi\phi_i}, \tag{3.1}$$

where t represents time, and c_i and ϕ_i $(0 \leq \phi < 2)$ are the amplitude and the phase for the i^{th} transition, respectively. Furthermore, $\psi_{\sigma_i}^{\alpha_i}(t-\tau_i)$ shows a translated (τ_i) and scaled (σ_i) source wavelet ψ, which is fractionally differentiated $(\alpha < 0)$ or integrated $(\alpha > 0)$. The seismic source wavelet ψ can be any arbitrary wavelet that satisfies the required conditions listed earlier in the discussion on seismic source functions. The parameters of interest, which we will hereafter refer to as attributes, in this case are the amplitude c_i, the location τ_i, the scale σ_i, the singularity order α_i, and the phase ϕ_i. Given the above representation, we present a new method, where the characterization problem is divided into two subproblems, namely detection stage, where the main events in the seismic data are located and extracted, and estimation stage, where the attributes for each individual waveform (event) are extracted by a nonlinear parametric inversion. Although we deal with discretized finite signals in our implementation, we use continuous signal notation interchangeably.

3.1 Detection by multiscale analysis

The purpose of the detection step is to find the singularities (major events) in the seismic trace. The detection problem does not fit straightforwardly into the classical deconvolution framework due to the existence of fractional-order transitions in the subsurface. The variety of the singularity orders

calls for a seismic-event-detection technique that does not make specific assumptions regarding the type of the transitions, e.g., spikes as for zero-order discontinuities. The continuous (complex) wavelet transform offers a multiscale edge (point singularity) detection approach (Mallat, 1997) that is robust for different waveforms, reflecting different types of transitions. Other than detecting the main events, this technique serves as a prior estimate for nonlinear parametric inversion.

A wavelet is a function $\varphi \in L^2(\mathbb{R})$ with zero average. The *complex wavelet transform* of a seismic trace s can be written as a convolution product

$$\mathcal{W}s(t,\sigma) = \big(s * \bar{\varphi}_\sigma\big)(t), \tag{3.2}$$

where $\bar{\varphi}_\sigma(t) = \frac{1}{\sqrt{\sigma}}\varphi^*(\frac{-t}{\sigma})$, and $\sigma \geq 0$ is the scale of wavelet. Here, the symbol * denotes the complex conjugate. In the wavelet domain, the point (t_0, s_0) such that $|\mathcal{W}s(t,\sigma_0)|$ is locally maximum at $t = t_0$ is referred to as modulus maximum. This maximum implies

$$\frac{\partial \mathcal{W}s(t,\sigma_0)}{\partial t} \mid_{t=t_0} = 0,$$

and should be a strict local maximum in either half- neighborhood of t_0 to avoid having several local maxima when $|\mathcal{W}s(t,\sigma_0)|$ is constant. Following Mallat (1997), we define Wavelet transform *modulus maxima line* (WT-MML) as a connected curve, $\sigma(t)$, in time-scale plane (t,σ), along which all points are modulus maxima. Singularities (events) are detected by finding the maximum point along each modulus maxima line (see Fig. 3.1(b)). These points yield approximate estimates for the scale (= bandwidth) and location of the reflection events. An initial approximation for the phase of the event is also provided by the phase of the complex wavelet coefficients, i.e., $\arg\{\mathcal{W}s(t,\sigma)\}$, at these points. This information is then used to build windowing functions used for the purpose of segmentation.

3.2 Segmentation

The result of the detection stage is a set of locations, scales, and phases, i.e., $\{(\tau^{(n)}, \sigma^{(n)}, \phi^{(n)}) \mid n = 1 \cdots N\}$, where N is the number of detected maxima. In order to extract the n^{th} detected waveform, we multiply the original seismic trace by a specific window function. The segmented events are given by

$$s^{(n)}(t) = \mathbf{W}(\tau^{(n)}, \sigma^{(n)})s(t) \quad \text{with} \quad n = 1 \cdots N, \tag{3.3}$$

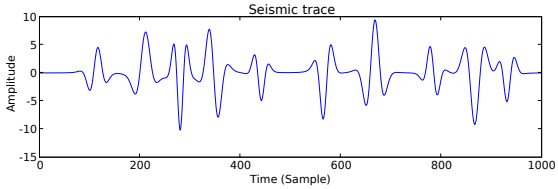

(a)

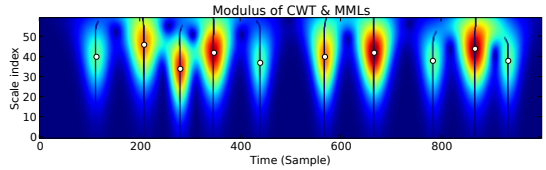

(b)

Figure 3.1: A typical example for detection stage of a synthetic seismic trace **(a)** with $k = 11$ reflection events. Wavelet coefficients for the signal are plotted in **(b)** with warm colors corresponding to large magnitudes. The vertical and horizontal axes show scale and location, respectively. Modulus maxima lines are shown as dark blue lines where white circles identify the scale and the location for the corresponding events.

where $\mathbf{W}(.)$ is the windowing operator centered at $\tau^{(n)}$, and has a support proportional to $\sigma^{(n)}$ (see Fig. 3.2).

The outputs of this procedure are N signals with 'isolated' events. Even though this segmentation procedure is somewhat arbitrary (e.g. it depends on a width parameter), we found this method to perform reasonably well for cases where inter-event distances are large enough (see Dossal and Mallat (2005) for more details). Sub-wavelength details are not extracted and are left to the ensuing estimation stage.

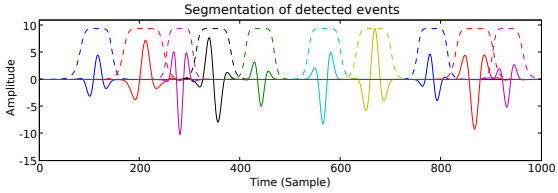

Figure 3.2: Partitioning of detected events for the synthetic seismic trace in Figure 3.1. Each individual event (solid waveform) is extracted by using a window function (dashed line with same color) centered at $\tau^{(n)}$ and a width proportional $\sigma^{(n)}$.

3.3 Nonlinear parametric inversion

In order to complete the characterization, we need to estimate attributes for the individual windowed waveforms $s^{(n)}(t)$ given by the detection stage. These isolated events are subjected to a nonlinear parametric inversion, where prior estimates on location, scale, and phase, are provided by the detection stage. To setup this procedure, we first need to refine our mathematical model for the parametrized waveforms in equation 3.1. We derive our model from a Gaussian bell-shaped waveform.

3.3.1 Parametric representation

Each element of the parametric family, also known as a manifold, is given by a fractional derivative/integration of the shifted and scaled Gaussian with some phase rotation. In the time domain, these waveforms are defined by a nonlinear function, $f_\theta : \mathbb{R}^5 \mapsto \mathbb{R}$, given by

$$f_\theta(t) = D^\alpha \left(\frac{1}{\sqrt{2\pi\sigma^2}} \, e^{(t-\tau)^2/2\sigma^2} \right) e^{j\pi\phi}, \tag{3.4}$$

with $\theta = [\tau, \sigma, \alpha, \phi]$ the set of parameters and D^α the α-order integration operator. Here, we denote location, scale, singularity order, and phase by τ, σ, α, and ϕ, respectively. Motivated by the work of Wakin et al. (2005), we can define the manifold as

$$M[\theta] = \{f_\theta : \theta \in \mathbf{\Theta}\},$$

where $\mathbf{\Theta}$ is the feasible parameter space. We will later show that $M[\theta]$ is a smooth manifold, i.e., it is differentiable with respect to its parameters (θ). We also assume that the relation $\theta \mapsto f_\theta$ is a one-to-one mapping. The nonlinear estimation procedure for each windowed waveform $s^{(n)}(t)$ consists of finding the best-matched element of the family, which is equivalent to solving the following minimization problems

$$\tilde{\theta}^{(n)} = \arg\min_{\theta \in \mathbf{\Theta}} \left\| s^{(n)} - M[\theta] \right\|_2^2 \quad \text{with} \quad n = 1 \cdots N, \tag{3.5}$$

where the objective function represents mismatch residual. Here, $\tilde{\theta}^{(n)}$ signifies the estimated attributes with $\tilde{}$ symbol denoting the approximation in values. To solve the above optimization problem, the BFGS quasi-Newton method (Nocedal and Wright, 1999; Kelley, 1999) is employed. In quasi-Newton methods, one does not need to compute the second derivatives of the objective function for the Hessian matrix. Instead, the Hessian is updated by analyzing successive gradients. Alternatively, a trust region method with the Levenberg-Marquardt parameter (Kelley, 1999) can be used to solve the minimization problem. As with the BFGS method, trust region methods also require the manifold to be smooth. This requirement suggests for a formulation in the frequency domain where the fractional derivatives are known analytically. The elements of the Gaussian waveform family in the frequency domain are now given by (Blu and Unser, 2003)

$$\hat{f}_\theta(\omega) = (j\omega)^{-\alpha/2+\phi} \; (-j\omega)^{-\alpha/2-\phi} \; e^{-\frac{(\sigma^2\omega^2)}{2}} \; e^{-j\omega\tau}, \tag{3.6}$$

where ω is the frequency. $\hat{f}_\theta(\omega) = \mathcal{F}(f_\theta(t))$ represents Fourier transform of $f_\theta(t)$ where $\mathcal{F}(.)$ is Fourier operator. One can show that the first two terms, which are responsible for both the fractional differentiation/integration and phase shift, are equivalent to $\omega^{-\alpha} \; e^{(j\pi\phi)}$. Analytical expressions for partial derivatives of the manifold in the frequency domain are given by

$$\begin{array}{rclcrcl} \dfrac{\partial}{\partial\tau} \; \hat{f}_\theta(\omega) & = & -j\omega \; \hat{f}_\theta(\omega), & & \dfrac{\partial}{\partial\alpha} \; \hat{f}_\theta(\omega) & = & -\ln(\omega) \; \hat{f}_\theta(\omega), \\ \dfrac{\partial}{\partial\sigma} \; \hat{f}_\theta(\omega) & = & -\sigma\omega^2 \; \hat{f}_\theta(\omega), & \text{and} & \dfrac{\partial}{\partial\phi} \; \hat{f}_\theta(\omega) & = & j\pi \; \hat{f}_\theta(\omega). \end{array} \tag{3.7}$$

The gradients for the mismatch error $e^{(n)}$ are then given by

$$J_i^{(n)} = \frac{\partial e^{(n)}}{\partial \theta_i} = 2\left\langle s^{(n)} - M[\theta], \gamma_{\theta_i} \right\rangle \quad \text{with} \quad \theta_i \in \theta, \tag{3.8}$$

where $\gamma_{\theta_i} = \frac{\partial f_\theta}{\partial \theta_i}$, and $\langle ., . \rangle$ denotes inner product of two signals. One can also think of $J_i^{(n)}$ as the projected estimation error for each parameter. The *Jacobian* matrix is given by $\mathbf{J}^{(n)} = \{J_i^{(n)} : i = 1 \cdots 4\}$.

Figure 3.3 shows the parameter estimation results for a single isolated event, where the BFGS method provides an acceptable solution to the minimization problem after only a few iterations. Figure 3.4 compares the estimated values of the singularity order with actual values. It also shows the fairly small mismatch between the original trace and the reconstructed trace by superposition of the estimated waveforms. We found the inversion results for the isolated events to be independent of noise below a reasonable level.

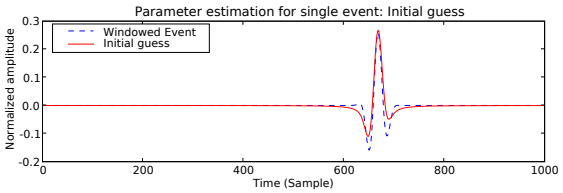

(a)

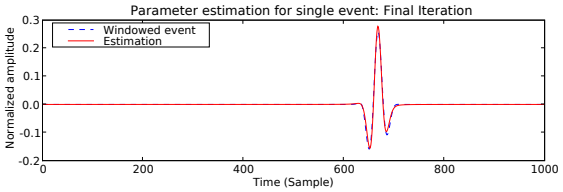

(b)

Figure 3.3: Parameter estimation for an individual event in Fig. 3.2. **(a)** Initial iteration of parameter estimation for the isolated event where dashed blue line shows windowed event and solid red line shows our guess. **(b)** Final iteration of parameter estimation for the isolated event where the estimated waveform matches the actual event.

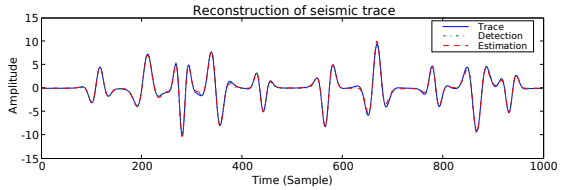

(a)

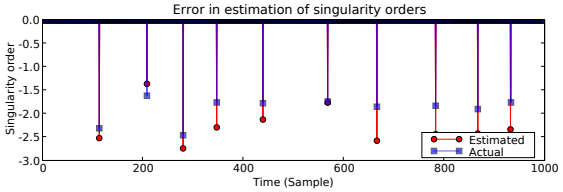

(b)

Figure 3.4: Characterization results for the synthetic trace in Figure 3.1. **(a)** Estimated seismic trace is formed by superposition of all characterized events and compared with the original seismic trace. **(b)** The estimated attributes of events (τ, α) are compared to their actual values.

Chapter 4

Attribute analysis

To characterize the major singularities in our marine data-set from west Shetlands, the detection-estimation method is applied to each trace of the time-migrated 2-D seismic image individually. The results are summarized in Figures 4.1, 4.2, and 4.3, where the vertical axis corresponds to the two-way travel time and horizontal axis shows lateral position. Although there are trace-to-trace variations, major features in the original image are captured and reconstructed quite accurately (see Fig. 4.1). Figure 4.2(a) shows the modulus of the detected events, which is directly related to corresponding reflectors' strength. Despite the existence of a relatively strong reflection at approximately $t = 2.9s$ (see Fig. 4.2(a)), there is only a slightly difference in the amplitudes of the reconstructed waveforms when compared to the real ones (cf. Fig. 4.1(a) and 4.1(b)).

Aside from localized estimates of the reflector strength, our characterization also provides localized estimates for scale, singularity order, and phase attributes (see Figures 4.2(b) and 4.3). The estimated values of the different attributes (color code) are plotted in Figures 4.2 and 4.3, overlaying the original seismic image (gray scale). The singularity order predicts the local regularity of the imaged reflectors; the sharper the transition, the more negative the order of singularity. As reported in the literature, the estimated singularity orders only express relative changes in the abruptness of the reflectors since they contain a contribution of the seismic source wavelet. The contribution is given by $\alpha = \alpha_{src} + \alpha_{abs}$, where α_{src} shows the singularity order for the seismic source wavelet and α_{abs} is the absolute singularity order associated with the imaged reflectors. As opposed to singularity orders which are relatively insensitive to dispersion (Herrmann and Stark, 2000), estimates for the scale increase for deeper reflections. This observation is consistent with dispersion, which leads to smaller values for scale, i.e., the ratio bandwidth over central frequency ($\frac{\Delta\omega}{\omega_0}$). Aside from dispersion effects, changes in the estimated scale also depend on the characteristic scale of the transitions. Finally, the phase attributes correspond to localized estimates for the instantaneous phase. As reported in the literature, this attribute allows us to distinguish between causal (coarsening upwards), anti-causal

(fining upwards), and lobe-shaped transitions (Dessing, 1997), while estimates for the singularity orders help us to discriminate between "thin layer sequences" ($-1 \leq \alpha_{abs} < 0$), caused by acoustic impedance variations that return to their initial value and step-like variations ($0 \leq \alpha_{abs} < 1$) where the initial and transition values differ. The difference for the corresponding singularity orders can be explained in terms of the well-known bright spots and local phase rotations associated with tuning of sub-wavelength layer thicknesses. In that case, the opposite sign reflectors act as a differentiator effectively, reducing the order of the transition by one.

Other than giving us a trust in our characterization method, lateral consistency of attributes along reflectors, as in Figure 4.2(b) and 4.3(a), has also important consequences for the interpretation of geological boundaries. Variety of estimated singularity orders for different stratigraphical horizons suggests that there exist an aggregation of varying order transitions other than zero-order steps and first-order ramp functions in the sedimentary basin. Additionally, it admits the existence of a link between the attribute values and type of the corresponding transitions. Accordingly, layer boundaries can no longer be considered as strictly local, as in the case for jump discontinuities. In the next section, we attempt to provide further lithology insights by zooming into the strong reflection event, where the estimated attributes show interesting behavior along the reflector.

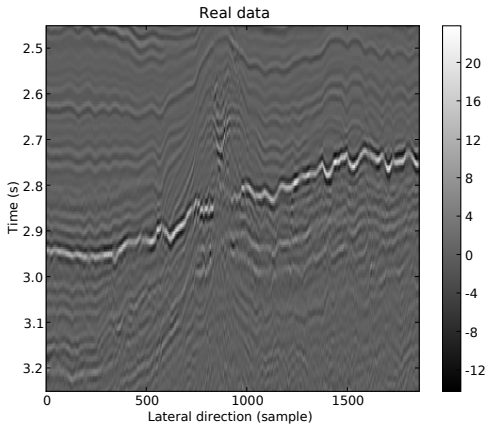

(a)

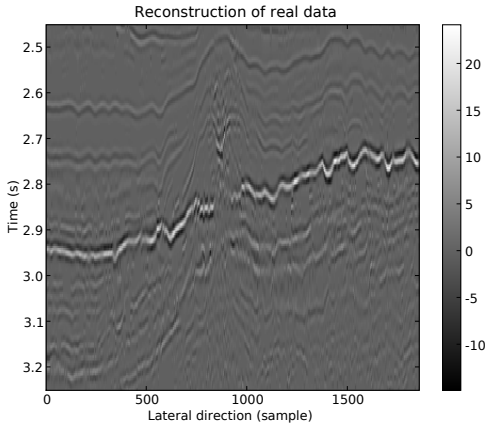

(b)

Figure 4.1: Reconstruction of real marine data recorded in west of Shetlands. **(a)** Imaged reflection amplitudes. **(b)** Trace-by-trace reconstruction of real data through superposition of all matched elements of the manifold.

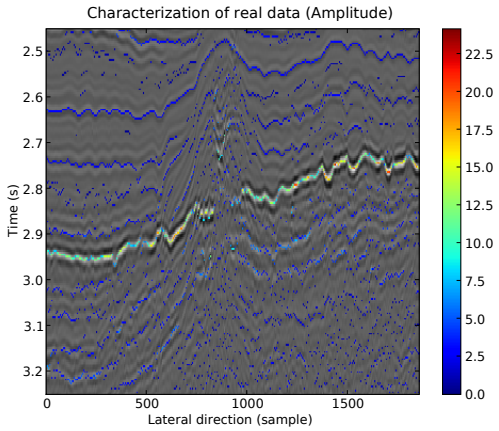

(a)

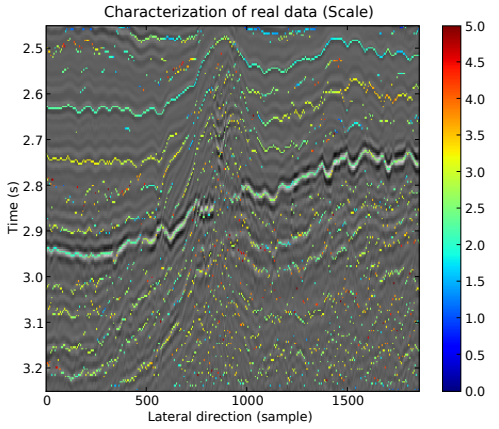

(b)

Figure 4.2: Estimated attributes for real data given in 4.1(a). The scatter plot of **(a)** amplitudes of reconstructed events, **(b)** estimated scale attributes overlays the gray scale imaged section. Warm colors in (a) and (b) show higher amplitudes and larger scales, respectively. The structure of detected events is nicely aligned with reflectors.

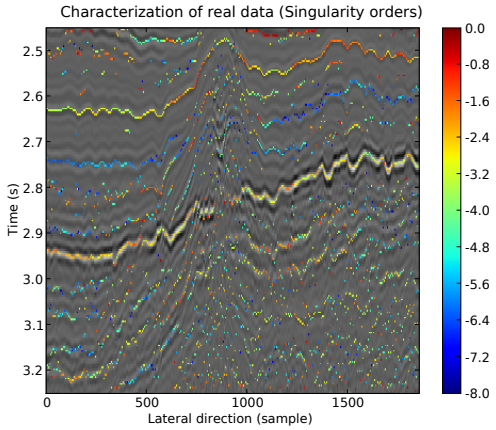

(a)

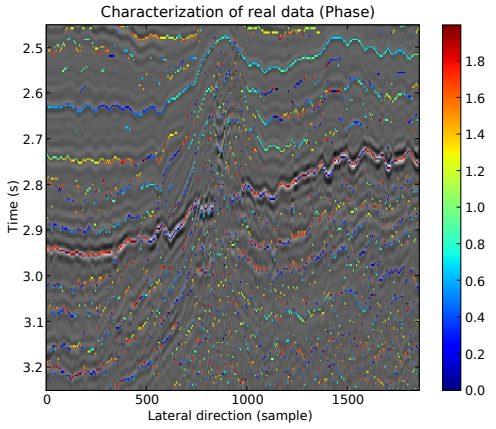

(b)

Figure 4.3: Estimated attributes for real data given in 4.1(a). The scatter plot of estimated **(a)** singularity order, and **(b)** instantaneous phase attributes overlays the gray scale imaged section. Warm colors in (a) show less sharp transitions.

Chapter 5

Opal-A to opal-CT transition and well-seismic tie

The seismically imaged region in Figure 4.1(a) represents a subsection of the Faeroe-Shetland basin, where a commercial exploration well was drilled for direct lithological calibration in 1999. Analysis of samples taken from the borehole revealed that the strong high-amplitude event, at $t = 2.9s$ in the seismic section, represents a diagenetic event corresponding to the opal-A (Amorphous) to opal-CT (Cristobalite/Tridymite) transition (Davies et al., 2001; Davies and Cartwright, 2002). The primary deposition of opals is largely due to biogenic processes during which minute marine organisms with siliceous skeletons, including sponges, settle to the bottom of sea after dying. The remains of these animals form non-crystalline opal (opal-A). Interestingly, this form of opal is reported to gradually transform to opal-CT as a result of silica diagenesis, which is due to the increasing overburden pressure in sedimentary rocks. In the second part of our study on the west Shetlands dataset, we are concerned with extracting more information on the lithological characteristics of stratigraphy that we know to exist. In this section, we zoom into the strong reflection present in the seismic image that corresponds to the diagenetic transition of opal-A to opal-CT. We will present an example of how these attributes can help us to interpret microscale transitions.

The diagenetic reflector starts at approximately $t = 2.9s$ (left) and progresses to $t = 2.7s$ (right). The estimated attributes remain relatively constant along this reflector although the seismic amplitudes vary significantly. Studies on the cuttings of the well have revealed that the volume fraction of opal-CT changes from 10% to 76% along the boundary (Davies and Cartwright, 2002). Assuming a linear gradient of the volume fraction, we use our site percolation model to build an elastic profile as a function of the volume fraction. For this purpose, elastic properties of opal-A and opal-CT are required as inputs for the percolation model. Since there are no well measurements (sonic and density) available near the diagenetic transition, representative values of elastic moduli for both opal types are taken from

the literature (Guerin, 2000, logs measured in hole 904A).

In Figure 5.1, elastic profiles for the transition according to the percolation model are depicted, where the modeled singularity is clearly visible in the velocity difference and hence the corresponding reflection coefficient sequence. Next, a synthetic seismic trace is generated according to the convolution model. Because the seismic source signature is unknown, we estimate the seismic source function with an average of sea bottom waveforms.

As stated earlier, the seismic source function is modeled by a Gaussian waveform parametrized by $[\sigma, \alpha_{src}, \phi] = [2.21, -3.78, 1.55]$ (cf. Eq. 3.6). The location and shape of the modeled seismic event (Fig. 5.2), given by convolution of the reflection coefficients with the source function, is controlled by the critical volume fraction p_c and singularity order β parameters of the percolation model. This will enable us to make a well-seismic tie, where we associate the singularity order α_{abs} with the β model by applying the detection-estimation method to the semi-synthetic seismic section (see Fig. 5.3(a)). For this purpose, we will try to find the best fit of the attributes for the real and synthetic part of the seismic reflector for varying β values. Figure 5.3(a) shows the results with matched orders, which correspond to $\beta = 0.81$ in the percolation model. The singularity order for the synthetic event (in the middle of section) is perfectly matched to an average value of orders for adjacent real traces. Since α_{abs} and β represent the same attribute from different perspectives, we expect α_{abs} for the diagenetic reflector to have the same value as β. However, there is a slight difference in the values of $\alpha_{abs} = \alpha - \alpha_{src} = 0.79$ and $\beta = 0.81$ due to the averaging approximation. Aside from a good match, The values of estimated phase attributes (see Fig. 5.3(a)) for the diagenetic event, which is about zero or 2π, show the causality of waveform associated with the event.

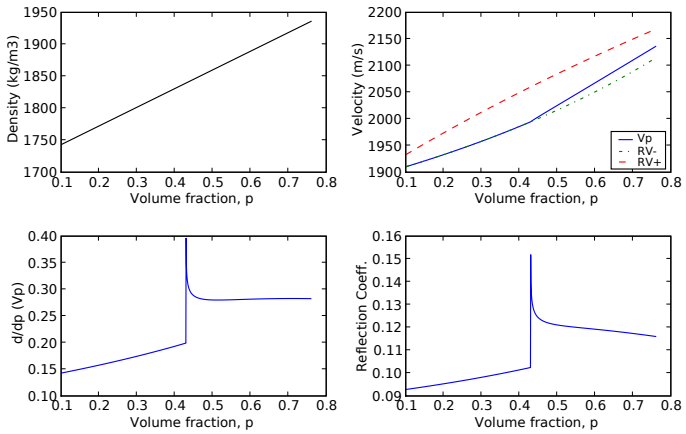

Figure 5.1: The site percolation model for the diagenetic transition of opal-A to opal-CT. Properties for opal-A are taken to be $\rho = 1713.90\ kg/m^3$ and $V_p = 1889.65\ m/s$. For opal-CT, density and P-wave velocity are assumed to be $\rho = 2006.06\ kg/m^3$ and $V_p = 2237.71\ m/s$, respectively. Density **(top left)** and P-wave velocity **(top right)** profile of the transition is determined as a function of volume fraction of opal-CT. The velocity, bounded by Reuss and Voigt averages, is showing a switch-like behavior at a critical point. The singularity is clearly visible from derivative of velocity **(bottom left)**, and also preserved in reflection coefficients **(bottom right)**.

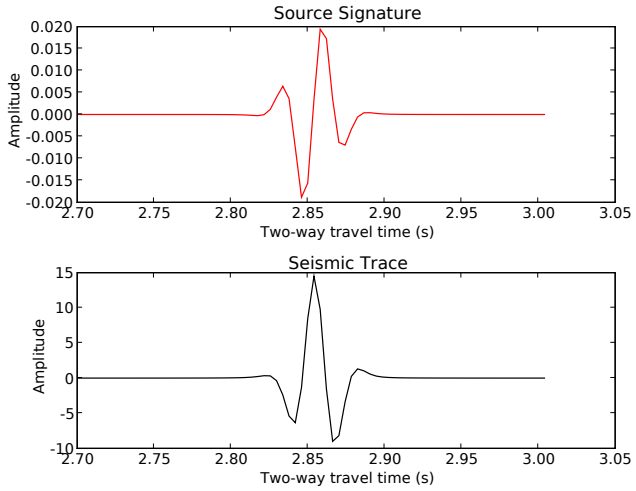

(a)

Figure 5.2: Synthetic data generation by convolution model; We estimate seismic source signature from sea bottom by using seismic waveform characterization. By taking an average over reconstructed waveforms for sea bottom seismic reflector, we estimate the seismic source function by a parametrized Gaussian waveform where $[\sigma, \alpha, \phi] = [2.21, -3.78, 1.55]$ **(top)**. **(bottom)** Synthetic trace is generated by convolution of reflection coefficients given in Figure 5.1 with the seismic source. Location and shape of the synthetic trace is a function of parameters of the site percolation model.

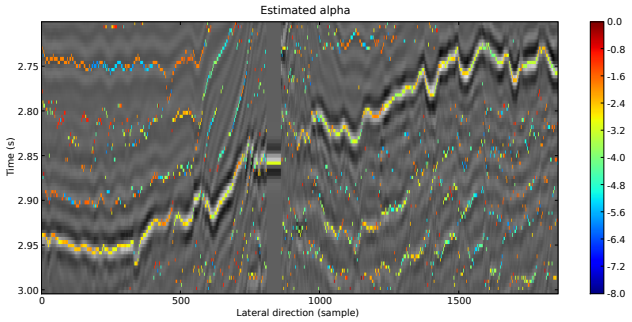

(a)

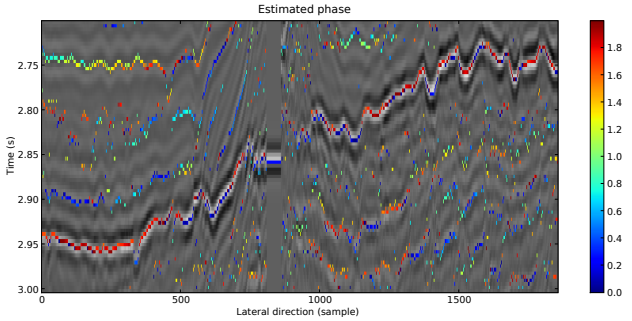

(b)

Figure 5.3: Well-seismic tie. By choosing the appropriate p_c value, diagenetic event is aligned in both synthetic traces (in the middle of section) and neighboring real traces. The detection-estimation method is applied to this semi-synthetic section in order to see how constraints from seismic waveforms fit with the ones from lithology. Estimated **(a)** singularity orders and **(b)** phase attributes are matched along the diagenetic event when $\beta = 0.81$.

Chapter 6

Discussion and Conclusions

In this thesis, we proposed a new approach to obtain lithological insights from seismic data in which we model a wider class of transitions from both lithological perspective (e.g. transitions from smooth connectivity in composition) and mathematical representation perspective, i.e., fractional-order discontinuities. This generalization provides us with more accurate and improved understanding of the subsurface geology.

The waveform characterization implies a representation for the geological record; where the detection stage extracts basic stratigraphy and estimation stage reveals the lithology of the subsurface. The singularity order and phase attributes especially, provide useful information on lithofacies. The former measures the transition sharpness and the latter can be used as a tool to distinguish between fining/coarsening upwards or lobe-shaped sequences. The characterization results on real data show a good alignment between the location of detected waveforms and seismic reflectors. As discussed earlier, the observed type of variations of attributes suggests that our parametric representation can provide us with constraints on the lithological boundaries. We have also answered the second question posed in the introduction part by finding the link between characterization attributes and corresponding lithological transition for the known diagenetic transition.

Finally, the bottleneck of our seismic characterization method is the segmentation, which is somewhat arbitrary. Although we choose a smooth window function, segmentation step can still cause some edge distortion for individual waveforms. Despite the fact that the estimation step assumes an accurate detection and windowing, the parametric inversion is able to reconstruct the distorted waveforms correctly in most cases. The segmentation problem is more probable when the events are very close to each other. Some studies are in progress to show that a specific minimum distance between different events is required in order to have an accurate recovery, i.e., precise separation of the two events. Consequently, very close events are not distinguishable and may be interpreted as one event with more negative (smaller) singularity order.

Bibliography

Benveniste, Y., 1987, A new approach to the application of mori-tanakas theory in composite materials: Mechanics of Material., **6**, 147 – 157.

Blu, T. and M. Unser, 2003, A complete family of scaling functions: the (α, τ) fractional splines: Proceedings of the Twenty-Eighth IEEE International Conference on Acoustics, Speech, and Signal Processing (ICASSP'03), 505 – 508.

Davies, R. J. and J. Cartwright, 2002, A fossilized opal a to opal c/t transformation on the northeast atlantic margin: support for a significantly elevated palaeogeothermal gradient during the neogene?: Basin Research, **14**, 467 – 486.

Davies, R. J., J. Cartwright, J. Pike, and C. Line, 2001, Early oligocene initiation of north atlantic deep water formation: Letters to Nature, **410**, 917 – 920.

Dessing, F., 1997, A Wavelet Transform Approach to Seismic Processing: PhD thesis, Delft University of Technology.

Dossal, C. and S. Mallat, 2005, Sparse spike deconvolution with minimum scale: Proceedings of Signal Processing with Adaptive Sparse Structured Representations, 123 – 126. (http://spars05.irisa.fr/ACTES/PS2-11.pdf).

Guerin, G., 2000, Acoustic and thermal characterization of oil migration, gas hydrates formation and silica diagenesis: PhD thesis, Columbia University.

Harms, J. C. and P. Tackenberg, 1972, Seismic signatures of sedimentation models: Geophysics, **37**, 45 – 58.

Hashin, Z. and S. Shtrikman, 1962, On some variational principles in anisotropic and nonhomogeneous elasticity: Journal of the Mechanics and Physics of Solids, **10**, 335 – 342.

Herrmann, F. J., 1997, A Scaling Medium Representation, a Discussion on Well-Logs, Fractals and Waves: PhD thesis, Delft University of Technology.

———, 1998, Multiscale analysis of well- and seismic data: Mathematical Methods in Geophysical Imaging V, SPIE, **3453**, 180 – 208.

———, 2001, Multi- and monoscale attributes for well- and seismic data: Chapter in the annual report of the Borehole Acoustics and Logging and Reservoir Delineation Consortia at MIT.

———, 2005, Seismic deconvolution by atomic decomposition: A parametric approach with sparseness constraints: Integr. Computer-Aided Eng., **12**, 69 – 91.

Herrmann, F. J. and Y. Bernabé, 2004, Seismic singularities at upper mantle discontinuities: a site percolation model: Geop. J. Int., **159**, 949 – 960.

Herrmann, F. J., W. J. Lyons, and C. Stark, 2001, Seismic facies characterization by monoscale analysis: Geophysical Research Letters, **28**, 3781 – 3784.

Herrmann, F. J. and C. Stark, 2000, A scale attribute for texture in well- and seismic data: Presented at the Soc. Expl. Geoph.

Holschneider, M., 1995, Wavelets an analysis tool: Oxford Science Publications.

Kelley, C. T., 1999, Iterative methods for optimization. Frontiers in Applied Mathematics, No. 18: SIAM.

Luo, H. and G. Weng, 1987, On eshelbys inclusion problem in a threephase spherically concentric solid and a modification of mori-tanakas method: Mechanics of Material, **6**, 347 – 361.

Mallat, S., 1997, A wavelet tour of signal processing: Academic Press.

Mori, T. and K. Tanaka, 1973, Average stress in matrix and average elastic energy of materials with misfitting inclusions: Acta Metallurgica, **21**, 571 – 574.

Muller, J., I. Bokn, and J. L. McCauley, 1992, Multifractal analysis of petrophysical data: Annales Geophysicae, **10**, 735 – 761.

Nocedal, J. and S. J. Wright, 1999, Numerical optimization, 1st ed. Springer Series in Operations Research: Springer-Verlag.

Payton, C., ed., 1977, Seismic stratigraphy - applications to hydrocarbon exploration, chapter Stratigraphic models from seismic data. AAPG.

Saggaf, M. M. and E. A. Robinson, 2000, A unified framework for the deconvolution of traces of nonwhite reflectivity: Geophysics, **65**, 1660 – 1676.

Wakin, M. B., D. L. Donoho, H. Choi, and R. G. Baraniuk, 2005, The multiscale structure of non-differentiable image manifolds: SPIE Wavelets XI, 413 – 429.

Yilmaz, Ö., 2001, Seismic data analysis: Society of Exploration Geophysicists.